UNIVERSITY OF AMSTERDAM

UvA-DARE (Digital Academic Repository)

CHIME/FRB Discovery and Localization of the Swift-observed FRB 20241228A

Curtin, Alice P.; Andrew, Shion; Simha, Sunil; Cai, Alice; Nimmo, Kenzie; Chatterjee, Shami; Cook, Amanda M.; Dong, Fengqiu Adam; Dong, Yuxin; Eftekhari, Tarraneh; Fong, Wen-Fai; Fonseca, Emmanuel; Hessels, Jason W.T.; Joseph, Ronniy C.; Kaspi, Victoria; Leung, Calvin; Main, Robert; Masui, Kiyoshi W.; Mckinven, Ryan; Michilli, Daniele; Ng, Mason; Pandhi, Ayush; Pearlman, Aaron B.; Sammons, Mawson W.; Sand, Ketan R.; Scholz, Paul; Shah, Vishwangi; Shin, Kaitlyn; Tohuvavohu, Aaron

DOI
10.3847/1538-4357/ae2ea0

Publication date
2026

Document Version
Final published version

Published in
Astrophysical Journal

License
CC BY

Link to publication

Citation for published version (APA):
Curtin, A. P., Andrew, S., Simha, S., Cai, A., Nimmo, K., Chatterjee, S., Cook, A. M., Dong, F. A., Dong, Y., Eftekhari, T., Fong, W.-F., Fonseca, E., Hessels, J. W. T., Joseph, R. C., Kaspi, V., Leung, C., Main, R., Masui, K. W., Mckinven, R., ... Tohuvavohu, A. (2026). CHIME/FRB Discovery and Localization of the Swift-observed FRB 20241228A. *Astrophysical Journal*, *998*(1), Article 97. https://doi.org/10.3847/1538-4357/ae2ea0

General rights
It is not permitted to download or to forward/distribute the text or part of it without the consent of the author(s) and/or copyright holder(s), other than for strictly personal, individual use, unless the work is under an open content license (like Creative Commons).

UvA-DARE is a service provided by the library of the University of Amsterdam (https://dare.uva.nl)

Disclaimer/Complaints regulations
If you believe that digital publication of certain material infringes any of your rights or (privacy) interests, please let the Library know, stating your reasons. In case of a legitimate complaint, the Library will make the material inaccessible and/or remove it from the website. Please Ask the Library: https://uba.uva.nl/en/contact, or a letter to: Library of the University of Amsterdam, Secretariat, P.O. Box 19185, 1000 GD Amsterdam, The Netherlands. You will be contacted as soon as possible.

Download date:17 Nov 2026

The Astrophysical Journal, 998:97 (11pp), 2026 February 10 https://doi.org/10.3847/1538-4357/ae2ea0
© 2026. The Author(s). Published by the American Astronomical Society.
OPEN ACCESS

CHIME/FRB Discovery and Localization of the Swift-observed FRB 20241228A

Alice P. Curtin[1,2,8], Shion Andrew[3,4], Sunil Simha[5,6], Alice Cai[5], Kenzie Nimmo[3], Shami Chatterjee[7], Amanda M. Cook[1,2,8], Fengqiu Adam Dong[9], Yuxin Dong[5], Tarraneh Eftekhari[5], Wen-fai Fong[5], Emmanuel Fonseca[10,11], Jason W. T. Hessels[1,2,8,12], Ronniy C. Joseph[1,2], Victoria Kaspi[1,2], Calvin Leung[13,14], Robert Main[1,2], Kiyoshi W. Masui[3,4], Ryan Mckinven[1,2], Daniele Michilli[15], Mason Ng[1,2], Ayush Pandhi[16,17], Aaron B. Pearlman[1,2], Mawson W. Sammons[1,2], Ketan R Sand[1,2], Paul Scholz[17,18], Vishwangi Shah[1,2], Kaitlyn Shin[3,4], and Aaron Tohuvavohu[19]

[1] Department of Physics, McGill University, 3600 rue University, Montréal, QC H3A 2T8, Canada; alice.curtin@mail.mcgill.ca
[2] Trottier Space Institute, McGill University, 3550 rue University, Montréal, QC H3A 2A7, Canada
[3] MIT Kavli Institute for Astrophysics and Space Research, Massachusetts Institute of Technology, 77 Massachusetts Ave, Cambridge, MA 02139, USA
[4] Department of Physics, Massachusetts Institute of Technology, 77 Massachusetts Ave, Cambridge, MA 02139, USA
[5] Center for Interdisciplinary Exploration and Research in Astronomy, Northwestern University, 1800 Sherman Avenue, Evanston, IL 60201, USA
[6] Department of Astronomy and Astrophysics, University of Chicago, William Eckhardt Research Center, 5640 S Ellis Ave, Chicago, IL 60637, USA
[7] Cornell Center for Astrophysics and Planetary Science, Cornell University, Ithaca, NY 14853, USA
[8] Anton Pannekoek Institute for Astronomy, University of Amsterdam, Science Park 904, 1098 XH Amsterdam, The Netherlands
[9] National Radio Astronomy Observatory, 520 Edgemont Rd, Charlottesville, VA 22903, USA
[10] Department of Physics and Astronomy, West Virginia University, PO Box 6315, Morgantown, WV 26506, USA
[11] Center for Gravitational Waves and Cosmology, West Virginia University, Chestnut Ridge Research Building, Morgantown, WV 26505, USA
[12] ASTRON, Netherlands Institute for Radio Astronomy, Oude Hoogeveensedijk 4, 7991 PD Dwingeloo, The Netherlands
[13] Department of Astronomy, University of California, Berkeley, CA 94720, USA
[14] Miller Institute for Basic Research, Stanley Hall, Room 206B, Berkeley, CA 94720, USA
[15] Laboratoire d'Astrophysique de Marseille, Aix-Marseille Univ., CNRS, CNES, Marseille, France
[16] David A. Dunlap Department of Astronomy and Astrophysics, University of Toronto, 50 St. George Street, Toronto, ON M5S 3H4, Canada
[17] Dunlap Institute for Astronomy and Astrophysics, University of Toronto, 50 St. George Street, Toronto, ON M5S 3H4, Canada
[18] Department of Physics and Astronomy, York University, 4700 Keele Street, Toronto, ON MJ3 1P3, Canada
[19] Division of Physics, Mathematics, and Astronomy, California Institute of Technology, Pasadena, CA 91125, USA
Received 2025 June 4; revised 2025 December 10; accepted 2025 December 15; published 2026 February 4

Abstract

On 2024 December 28, the Canadian Hydrogen Intensity Mapping Experiment (CHIME) FRB project detected the thus-far nonrepeating FRB 20241228A with a real-time signal-to-noise ratio of >50. Approximately 112 s later, the X-ray Telescope on board the Neil Gehrels Swift Observatory was on-source, the fastest follow-up to date of a nonrepeating fast radio burst (FRB). Using CHIME/FRB and two of the three CHIME/FRB Outriggers, we obtained a very-long-baseline interferometry (VLBI) localization for FRB 20241228A with a 1σ confidence ellipse of $11''$ by $0.''2$. This represents the first published localization using both the CHIME k'ni?atn k'l⌣stk'masqt and CHIME Green Bank Observatory Outriggers. We associate FRB 20241228A with a star-forming galaxy at a redshift of $z = 0.1614 \pm 0.0002$. The persistent X-ray luminosity limit at this source's location and distance is $<1.2 \times 10^{43}$ erg s^{-1} in the 0.3−10 keV band, the most stringent limit of any nonrepeating FRB to date. The stellar mass ($\sim 2.6 \times 10^{10}\, M_\odot$) and star formation rate ($\sim 2.9\, M_\odot$ yr^{-1}) of the host galaxy of FRB 20241228A are consistent with the broader FRB host-galaxy population. We measure significant scattering (∼1 ms at 600 MHz) and scintillation (∼15 kHz at 600 MHz) along the line of sight to this source, and suggest the scintillation screen is Galactic while the scattering screen is extragalactic. FRB 20241228A represents an exciting example of a new era in which we can harness VLBI localizations and rapid high-energy follow-up to probe FRB progenitors.

Unified Astronomy Thesaurus concepts: Radio transient sources (2008); Transient sources (1851); Radio bursts (1339); Very long baseline interferometry (1769); Radio interferometry (1346)

1. Introduction

Searching for high-energy counterparts to fast radio bursts (FRBs) is a promising avenue for constraining the nature of FRB progenitors. In 2020 April, the detection of an FRB-like burst associated with the Galactic magnetar SGR 1935+2154 strongly suggested that at least some FRBs arise from magnetars (C. D. Bochenek et al. 2020; CHIME/FRB Collaboration et al. 2020a). Interestingly, the radio burst from SGR 1935+2154 occurred at a time of increased X-ray activity (D. M. Palmer & Swift/BAT Team 2020), and was accompanied by simultaneous high-energy emission in both the X-rays and soft gamma rays (S. Mereghetti et al. 2020; C. K. Li et al. 2021; A. Ridnaia et al. 2021).

Observing similar high-energy emission from an extragalactic FRB would further support the connection between FRBs and magnetars. The detection would also provide critical insight into the total energy budget of FRBs, and might point to a connection with other classes of transients from similar progenitors, e.g., supernova explosions, gamma-ray bursts, and accreting X-ray binaries. However, no FRBs have been detected from other known Galactic magnetars (S. P. Tendulkar et al. 2016) or proposed magnetar flares (A. P. Curtin & CHIME/FRB Collaboration 2023). Furthermore, despite many

Original content from this work may be used under the terms of the Creative Commons Attribution 4.0 licence. Any further distribution of this work must maintain attribution to the author(s) and the title of the work, journal citation and DOI.

follow-up studies of FRB sites and cross-matching with known high-energy transients, there has been no significant detection or association of high-energy emission with an extragalactic FRB, e.g., in the optical (L. K. Hardy et al. 2017; D. Hiramatsu et al. 2023; C. D. Kilpatrick et al. 2024), X-ray (P. Scholz et al. 2017, 2020; M. Pilia et al. 2020; T. Eftekhari et al. 2023; A. M. Cook et al. 2024; A. B. Pearlman et al. 2025; Z. Yan et al. 2025), or gamma ray (S. Yamasaki et al. 2016; C. Casentini et al. 2020; A. P. Curtin et al. 2023, 2024). For FRB 20201124A, L. Piro et al. (2021) reported the detection of a faint, persistent X-ray source spatially coincident with the location of the FRB, but they concluded that the emission was consistent with that expected from star formation in the region.

Two key challenges in detecting high-energy emission from extragalactic FRBs are the small number of known repeaters and the stochastic nature of their activity. Only ∼3% of FRBs have been seen to repeat (CHIME/FRB Collaboration et al. 2023), and of those only one (FRB 20180916B) repeats with a definitive activity period (CHIME/FRB Collaboration et al. 2020b).[20] Thus, the coordination of high-energy observations at the time of a radio detection is extremely difficult. Some repeating sources show periods of high source activity, which have proved fruitful for high-energy follow-up with X-ray telescopes (P. Scholz et al. 2017; P. Scholz et al. 2020; M. Pilia et al. 2020; M. Trudu et al. 2023; A. M. Cook et al. 2024; A. B. Pearlman et al. 2025). However, for nonrepeating FRBs, similar observations have relied on serendipitous observations with wide-field X-ray telescopes at the times of FRBs (A. Anumarlapudi et al. 2020; C. Guidorzi et al. 2020; G. Waratkar et al. 2025), making simultaneous observations infeasible in most cases. Instead, extremely rapid follow-up observations are often required to be able to capture near-simultaneous multiwavelength emission.

The Canadian Hydrogen Intensity Mapping Experiment (CHIME) FRB project has detected nearly 5000 FRBs since its initial commissioning in 2018 (CHIME/FRB Collaboration 2026), with a daily FRB detection rate of 2−3 FRBs per day (CHIME/FRB Collaboration et al. 2018). CHIME/FRB is equipped with a VOEvent service to provide near-immediate (∼10 s) alerts after an FRB (E. Petroff et al. 2017; T. C. Abbott et al. 2025), key for rapid multiwavelength follow-up. This capability enables real-time coordination with telescopes like the Neil Gehrels Swift Observatory (N. Gehrels et al. 2004), which has an automatic repointing algorithm to ingest triggers such as CHIME/FRB's VOEvents (A. Tohuvavohu et al. 2020).

On 2024 December 28, CHIME/FRB detected a bright FRB with a real-time signal-to-noise ratio (S/N) of 50. The X-Ray Telescope (XRT) on board Swift immediately slewed to the source and was on target collecting photons within 112 s. Offline analysis determined an improved localization for the FRB,[21] and confirmed that the source was located within Swift/XRT's field of view (FOV). A. Tohavavohu et al. (2026, in preparation) present a detailed description of the Swift triggering process, as well as the persistent X-ray limit at the position of FRB 20241228A. Here, we present the CHIME/FRB Outriggers (CHIME/FRB Collaboration et al. 2025a) very-long-baseline interferometry (VLBI) localization for FRB 20241228A, along with the most probable host galaxy and redshift. This is the first FRB localization to include two of the three CHIME/FRB Outriggers, including the longest Outrigger baseline. We also discuss the burst morphology, with particular focus on the scintillation and scattering features present in the burst, and the nonrepeating nature of the source.

In Section 2, we introduce CHIME/FRB, the CHIME/FRB Outriggers, and present the VLBI localization. In Section 3, we discuss the most probable host galaxy associated with FRB 20241228A. We then discuss the burst morphology, and in particular a detection of scintillation within FRB 20241228A, in Section 4. We conclude in Section 5 by discussing the host galaxy, repetition rate, and scintillation features of the burst in the context of the broader FRB field.

2. Observations

2.1. CHIME/FRB Burst Discovery

CHIME is located near Penticton, British Columbia at the Dominion Radio Astrophysical Observatory. Consisting of four 100 × 20 m cylindrical, parabolic dishes, CHIME has a total FOV of ∼250 deg^2 (dependent on frequency; C. Ng et al. 2017). Each dish consists of 256 dual-polarization antennas operating between 400 and 800 MHz. FRB-like signals are searched for in total-intensity data at a time resolution of 0.983 ms. For events with S/N ratios greater than a specified cutoff (typically ≈12), we save the channelized raw voltage data (1024 frequency channelsl) at a time resolution of 2.56 μs. This allows for both improved localization of the event through offline beamforming (of order arcminutes, often referred to as a "baseband" localization; D. Michilli et al. 2021; CHIME/FRB Collaboration et al. 2024) as well as studies of the burst's polarization and morphology properties.

FRB 20241228A was detected by CHIME/FRB's real-time pipeline on 2024 December 28 at 15:55:56 UTC (topocentric at CHIME near Penticton, Canada), with a real-time S/N of 50.2 (see Figure 1). The real-time pipeline dispersion measure (DM) of the source was 246.3 ± 0.4 pc cm^{-3}. The maximum Galactic DM contribution in the direction of the event is 23.8 pc cm^{-3} in the NE2001 electron density model (J. M. Cordes & T. J. W. Lazio 2002) or 22.75 pc cm^{-3} in the YMW17 model (J. M. Yao et al. 2017), significantly below the source's DM and hence confirming its extragalactic nature. Despite 119 hr of exposure at this source's location (see Section 4.4), we have not yet observed any other candidate bursts from this source, i.e., any other events in our database that are (i) consistent on the sky with the position of FRB 20241228A, (ii) within 5 pc cm^{-3} of the DM, and (iii) above our nominal S/N threshold of 8. CHIME/FRB has some sensitivity to very bright bursts in our side lobes, i.e., we can detect bright bursts like Crab Pulsar giant pulses many degrees off meridian (e.g., H.-H. Lin et al. 2024). We performed the same database search along the apparent positional arc of FRB 20241228A, and found no plausible side-lobe repeats of the source. In short, FRB 20241228A is classified as a thus-far nonrepeater.

2.2. CHIME/FRB Outrigger Localizations

The CHIME/FRB Outriggers (herein referred to as the Outriggers) are a VLBI network of three CHIME-like

[20] K. M. Rajwade et al. (2020) also identified a candidate 157 days periodicity in FRB 20121102A.

[21] Due to CHIME's strong side lobes, real-time FRB localizations can span ∼5°−10° in R.A. and ∼1° in decl.

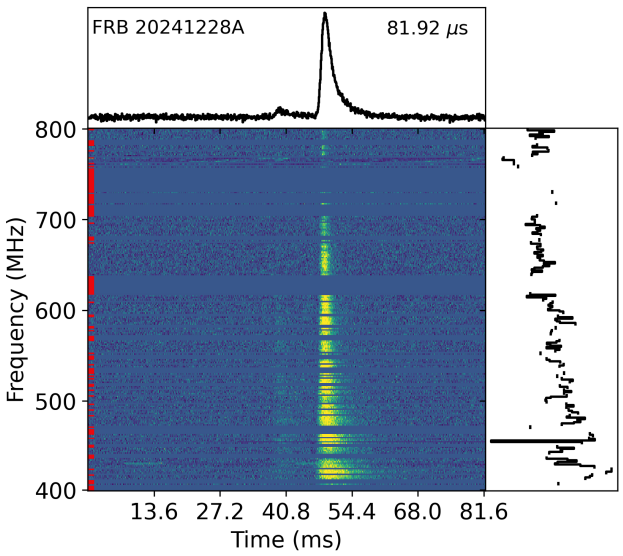

Figure 1. Dynamic spectrum for FRB 20241228A at a time resolution of 81.92 μs using raw voltage data. The time is relative to the fiducial arrival time of the burst. The data are scrunched in frequency by a factor of 4, for a resolution of 1.56 MHz. The top panel shows the frequency-summed time series, while the right panel shows the burst's spectrum averaged over both the burst and the surrounding noise. The ∼30 MHz ripple seen in the spectrum is not astrophysical and instead corresponds to reflections between the cylinders and the focal lines. Channels which are either flagged due to RFI or which are missing due to networking issues are indicated with red ticks.

cylindrical telescopes located across North America. With a maximum baseline of 3370 km, the Outriggers will localize hundreds to thousands of CHIME-detected FRBs to ∼50 mas precision (CHIME/FRB Collaboration et al. 2025a). The first Outrigger, k'ni?atn k'l⌣stk'masqt (KKO),[22] is located in British Columbia, 66 km west of CHIME, and provides improved localizations of order an arcsecond in R.A. (A. E. Lanman et al. 2024). The KKO Outrigger has already localized and identified the host galaxies for 21 FRBs (CHIME/FRB Collaboration et al. 2025b), and was the first to localize a repeating FRB to the outskirts of a quiescent galaxy (T. Eftekhari et al. 2025; V. Shah et al. 2025).

The second CHIME Outrigger is located at the National Radio Astronomy Observatory in Green Bank, West Virginia (hereafter CHIME-GBO) and, in conjunction with the CHIME-KKO baseline, provides 50 mas × 20″ localization capabilities. Because the CHIME-GBO baseline is nearly colinear with the CHIME-KKO baseline (see also Figure 2 of CHIME/FRB Collaboration et al. 2025a), a third Outrigger, located in Hat Creek, California at the Hat Creek Radio Observatory, is required to provide the *uv* coverage necessary for a full 2D localization of ∼50 × 150 mas. The Hat Creek Outrigger is presently under commissioning.

At the time of FRB 20241228A, both the KKO and GBO Outrigger stations were operating in full scientific mode. The HCO Outrigger was still undergoing final digital and analog deployment, and hence was not online. With a CHIME/FRB detection S/N greater than 15, FRB 20241228A triggered raw voltage data capture at CHIME, the KKO Outrigger, and the GBO Outrigger. FRB 20241228A thus represents the first localization using both the CHIME-KKO and CHIME-GBO baselines. A description of the CHIME-KKO system, as well as its localization capabilities, has already been given in detail in A. E. Lanman et al. (2024). Below, we provide a brief overview of the CHIME-GBO system and its astrometric capabilities. An in-depth description of the construction, calibration, and validation of the GBO Outrigger will be discussed in detail in a future paper.

The calibration and validation strategy for the GBO Outrigger has closely matched that for the KKO Outrigger. Bright, in-beam sources identified in our calibrator survey (S. Andrew et al. 2025) are observed commensally as delay calibrators for each of our long baselines (C. Leung et al. 2021). For KKO-detected FRBs, there are approximately 10 in-beam calibrators in a given FRB voltage dump. However, given the significantly longer baseline of GBO as compared to KKO, this number reduces to only two in-beam calibrators as many are resolved out in the longer baseline and/or are too faint to be detected. While GBO has a significantly larger collecting area KKO, the S/N is reduced along its baseline due to significant radio frequency interference (RFI) at site. A more detailed description of the S/N reduction on the CHIME-GBO baseline will be provided in future work.

We derive our error budget for this source from test localizations of ∼80 pulsars localized to milliarcsecond-level precision (VLBA/21A-314, PI: Kaczmarek; VLBA/22A-345, PI: Curtin; VLBA/23A-099, PI: Curtin; VLBA/24B-328, PI: Curtin; W. F. Brisken et al. 2002; S. Chatterjee et al. 2009; A. T. Deller et al. 2019; R. Lin et al. 2023) and over 200 International Celestial Reference Frame (ICRF) calibrators. For test localizations with similar target–calibrator separations (discussed below), the rms localization error on the CHIME-GBO baseline is smaller than 200 mas. Thus, we provide a final uncertainty of 200 mas along the CHIME-GBO baseline for this FRB's localization region. This error budget will be discussed further in future work.

We used the `pyfx` software (C. Leung et al. 2025) to form correlated visibilities between CHIME and the KKO and GBO Outriggers. FRB 20241228A was initially detected by CHIME/FRB with a real-time (at a time resolution of 0.983 ms) S/N of ∼50. After re-beamforming the data, the S/N is >200 at a time resolution of 0.655 ms. It was thus detected in the cross-correlated visibilities with a S/N of ∼45 along the CHIME-KKO baseline and with a S/N of ∼35 along the CHIME-GBO baseline. Two in-beam calibrators were detected in the voltage dumps at both KKO and GBO. For both baselines, we chose J143844.7+621154, the closer of the two, as our calibrator. Located 50° from FRB 20241228A, J143844.7+621154 was detected with a cross correlation S/N of 30.

In Figure 2, we show the 1σ and 3σ localization ellipses from the CHIME-GBO baseline overlaid on a Dark Energy Camera Legacy Survey (DECaLS; A. Dey et al. 2019) image at this location. The parameters for the ellipse are given in Table 1. As shown in Figure 3, the CHIME-KKO and CHIME-GBO baselines each provide 1D localizations that are primarily constrained along the east–west direction. Thus, the final uncertainty in the semiminor axis of the combined CHIME-KKO-GBO localization is significantly smaller than that of the semimajor axis. We note that for the final ellipse region (bottom panel of Figure 3), we have also incorporated

[22] The name of the first Outrigger, k'ni?atn k'l⌣stk'masqt, was a generous gift from the Upper Similkameen Indian Band and means "a listening device for outer space."

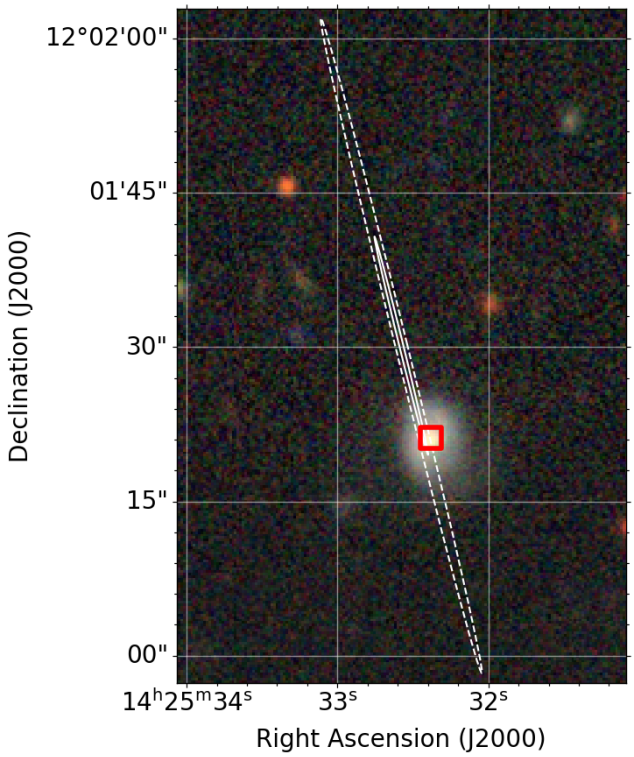

Figure 2. Joint localization (CHIME-GBO, CHIME-KKO, and CHIME/FRB baseband) on top of the DECaLS field for FRB 20241228A. The 1σ localization is shown with a white solid line, while the 3σ ellipse is shown with a white dashed line. The most probable host galaxy ($P(O|x) = 0.96$) is shown with a red square.

Table 1
Burst Localization

R.A.	Decl.	Seminminor Axis	Semimajor Axis	Position Angle
$14^h25^m32^s.58$	$12°01'30''.15$	$10''.93$	$0''.20$	$13°.805527$

Note. Parameters for the 1σ CHIME Outriggers VLBI localization ellipse for FRB 20241228A, with the center of the ellipse defined in the ICRS J2000 reference frame.

CHIME/FRB's baseband localization, which significantly constrains the localization in decl.

3. Host-galaxy Localization and Association

3.1. Host Association

To determine the most probable host galaxy of FRB 20241228A, we used the Probabilistic Association of Transients to their Hosts (or PATH) framework (K. Aggarwal et al. 2021). We utilize DECaLS to identify host-galaxy candidates in the field of FRB 20241228A down to a 5σ limiting r-band magnitude $m_r = 23.4$ mag (A. Dey et al. 2019). We adopt the default "inverse" prior to account for the larger number of faint galaxies and a prior probability that the host is unseen of $P(O|x) = 0.15$, motivated by the simulations of B. Andersen et al. (2026, in preparation). For the prior on the FRB offset distribution with respect to its host, we assume an underlying exponential distribution with a scale length equal to one-half the galaxy half-light radius. Using the FRB coordinates and

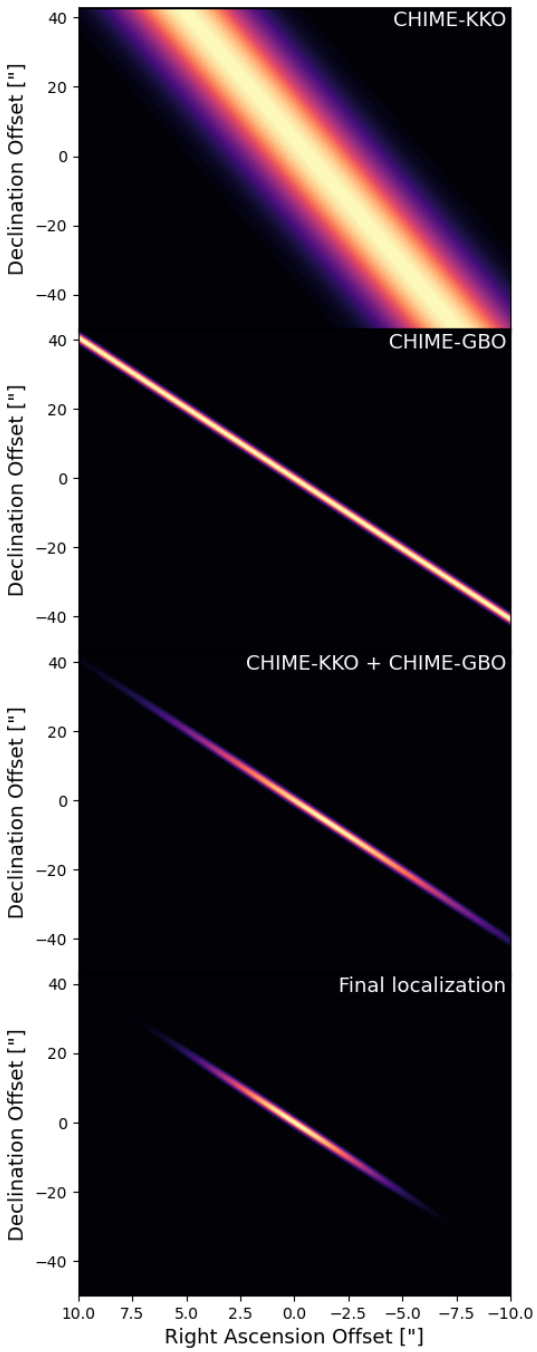

Figure 3. Top panel: probability map for the localization of FRB 20241228A using solely the CHIME-KKO baseline. The offsets in R.A. and decl. are relative to the center of the final localization ellipse. Lighter colors represent areas with higher localization probability. Middle top panel: same as first except for the CHIME-GBO baseline. Middle lower panel: combined localization using the CHIME-KKO and CHIME-GBO baselines. Due to the near colinear baselines of CHIME-KKO and CHIME-GBO, the resolving power from combining the two is largely along a single axis. Bottom panel: combined localization using the CHIME-KKO baseline, CHIME-GBO baseline, and CHIME/FRB baseband localization. The baseband data significantly constrains the final localization in decl.

ellipse parameters presented in Table 1, we identified the most likely host galaxy to have a posterior probability $P(O|x) = 0.96$. This is the only galaxy apparent in DECaLS that intersects the Outrigger position (see Figure 2). We obtain a position for the host galaxy of J142532.4s+120121.2.

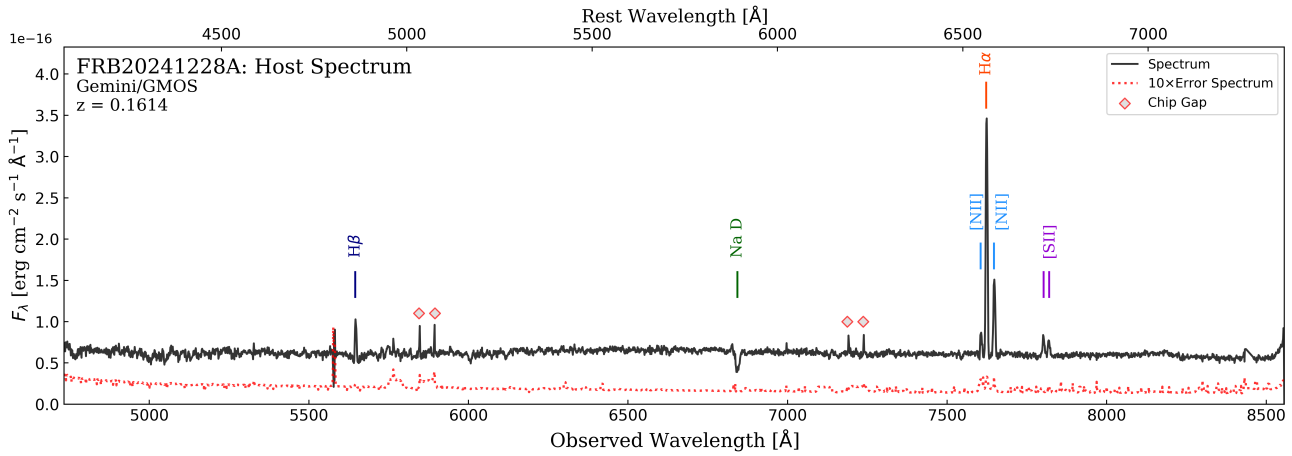

Figure 4. Gemini/GMOS spectrum of the most probable host galaxy of FRB 20241228A (black). Also plotted is the error spectrum (red dotted), which has been scaled by a factor of 10 for readability. The locations of observed spectral features which facilitated a redshift determination are indicated. False features induced by the detector chip gaps are marked by the red-bordered diamonds.

3.2. Spectroscopic Observations

Using the Gemini Multi-Object Spectrograph (GMOS) mounted on the 8 m Gemini-North telescope, we obtained optical spectroscopy of the host of FRB 20241228A on 2025 March 3 UT (PI: T. Eftekhari).[23] We took a total of 4 × 900 s exposures with a 1″ slit width using the B480 grating and the GG455 blocking filter at central wavelengths of 640 and 650 nm. We reduced and coadded the spectra using the Python Spectroscopic Data Reduction Pipeline (`PypeIt`, v1.16; J. X. Prochaska et al. 2020). We applied absolute flux calibration and a telluric correction to the spectra using a spectrophotometric standard star observation taken in the same spectral setups, and atmospheric model grids available in `PypeIt`.

To determine the redshift of the galaxy, we utilized the Manual and Automatic Redshifting (`Marz`) analysis software (S. Hinton et al. 2016). `Marz` performs a cross correlation between the measured spectra and various archetypal template models to determine both the broad galaxy type (e.g., whether dominated by emission lines or absorption features) and its redshift.[24] Applying `Marz` to the host galaxy of FRB 20241228A yields a redshift of $z = 0.1614 \pm 0.0002$. `Marz` does not report a redshift uncertainty, but we derive this from the 1σ width of the lines. The prominent spectral emission features (Hα, Hβ, S II) in the Gemini/GMOS spectrum (Figure 4) as well as the detection of this source in 1550 s of Galaxy Evolution Explorer (GALEX; P. Morrissey et al. 2007; L. Bianchi et al. 2017) near-UV (NUV) data (21.2 mag) indicate that the galaxy is star-forming (see Section 3.4). Deep far-UV (FUV) observations are not available from GALEX for this field (only 95 s of total integration available) but we visually identify a slight excess in photons at the location of the host. Within the DECaLS catalog, the galaxy has an r-band magnitude $m_r = 17.8$ and is best fit by a Sérsic profile.

3.3. Host-galaxy SED and Spectral Modeling

We use the Code Investigating GALaxy Emission (`CIGALE`) package (v. 2025.0; M. Boquien et al. 2019) to fit the host-galaxy spectral energy distribution (SED) and derive a stellar mass (see Figure 7 in the Appendix). Our input photometry spans the UV to far-IR, and is collated from the Panoramic Survey Telescope and Rapid Response System (Pan-STARRS; K. C. Chambers et al. 2016), Sloan Digital Sky Survey (SDSS; D. G. York et al. 2000), DECam Local Volume Exploration Survey (DELVE; A. Drlica-Wagner et al. 2021), DECaLS, and Wide-field Infrared Survey Explorer (WISE; E. L. Wright et al. 2010) databases. To correct the photometry for Galactic extinction, we assume $R_V = 3.1$ and query the IRSA dust extinction database at the FRB position,[25] and find $E(B-V) = 0.02$ (E. F. Schlafly & D. P. Finkbeiner 2011). We incorporate the filter transmission curves for each band from the Spanish Virtual Observatory filter database for our extinction correction calculations (C. Rodrigo & E. Solano 2020; C. Rodrigo et al. 2024). We additionally convert all magnitudes to the AB system where applicable. Following the methodology of S. Simha et al. (2020), we assume a delayed-exponential star formation history (SFH), a synthetic stellar population prescribed by G. Bruzual & S. Charlot (2003), a G. Chabrier (2003) initial mass function (IMF), dust attenuation models adapted from D. Calzetti (2001), and IR emission templates from D. A. Dale et al. (2014), where the active galactic nucleus fraction to the 5–20 μm emission was capped at 20%. For the host galaxy of FRB 20241228A, we find a best-fit stellar mass of $(2.6 \pm 0.3) \times 10^{10} M_\odot$ (68% confidence intervals).

3.4. Star Formation Rate Estimate

To estimate line fluxes from the GMOS spectrum and star formation rate (SFR) of the host, we use the `pPXF` package (M. Cappellari 2017) to fit the main nebular emission lines. We correct the line fluxes for Galactic reddening with the same method as previously explained for the photometry. We tabulate the extinction-corrected line fluxes in Table 2. Based on the observed Hβ/Hα flux ratio, and assuming an intrinsic atomic

[23] Spectroscopic data were collected by the Fast and Fortunate for FRB Follow-up Collaboration (https://www.frb-f4.org/) using the `FFFF-PZ` observation management tool, built and modeled after `YSE-PZ` (D. A. Coulter et al. 2022, 2023), and first implemented for FRBs in CHIME/FRB Collaboration et al. (2025b).

[24] We used the six standard galaxy templates for this cross correlation.

[25] https://irsa.ipac.caltech.edu/applications/DUST/

Table 2
Nebular Emission-line Fluxes for the Host of FRB 20241228A

Emission Line	Flux (10^{-16} erg s^{-1}cm^{-2})
Hα	20.8 ± 0.1
Hβ	3.94 ± 0.08
[N II] 6583	8.3 ± 0.1
[S II] 6716	1.61 ± 0.06
[S II] 6731	1.24 ± 0.06

Note. [O III] emission features were not detected from this galaxy and the [O II] doublet is outside the wavelength coverage. The reported fluxes are corrected for Milky Way dust extinction.

emission flux ratio of 2.87 (D. E. Osterbrock & G. J. Ferland 2006), we estimate an intrinsic reddening from the host galaxy of $A_V = 1.77$ mag. Subsequently, we estimate the Hα luminosity as $(5.79 \pm 0.03) \times 10^{41}$ erg s^{-1}. Assuming the R. C. Kennicutt (1998) relation for inferring SFR from Hα flux, and multiplying by 0.63 to convert to the Chabrier IMF (C. Conroy et al. 2009), we estimate the current host-galaxy SFR is $2.9 \pm 0.8\,M_\odot\,\mathrm{yr}^{-1}$ (30% scatter in the Kennicutt relation).

3.5. Galactocentric Offset

Following the method presented by A. C. Gordon et al. (2025), we determine the FRB's offset from the host-galaxy center by calculating the distance from each point in the FRB localization probability density function (pdf) to the galaxy center, weighted by the pdf value at that point. We find the FRB has an average galactocentric host-galaxy offset of 46^{+47}_{-32} kpc, in which the median and uncertainties have been calculated through weighting by the localization probability at every point within the ellipse. To determine the angular size of the host galaxy, we use the `GALFIT` software package (C. Y. Peng et al. 2002). We fit an elliptical isophote to the DECaLS r-band image of the host. The best-fit model gives a half-light radius of $2\farcs3 \pm 0\farcs2$. At a redshift of $z = 0.1614$, this corresponds to a physical size of 6.6 ± 0.6 kpc, assuming cosmological parameters from Planck Collaboration et al. (2020). In combination with the offset, this corresponds to a host-normalized offset (e.g., normalized by the size of the host) of $7^{+7}_{-5} r_e$ (where r_e is the effective radius). We caution that the uncertainties are very large here (although supportive of a nonzero offset), and hence do not further interpret this offset.

4. Burst Properties

4.1. Morphology

We follow the method outlined by K. R. Sand et al. (2025) and A. P. Curtin et al. (2025) to determine the morphological burst properties of FRB 20241228A. In particular, we employ the `fitburst` fitting algorithm, which assumes a given burst can be described using a set of exponentially modified Gaussians (E. Fonseca et al. 2024). `Fitburst` performs a joint 2D spectrotemporal fit that includes the burst's scattering timescale and DM, along with a per-subburst spectral index, spectral running, and width. In Table 3, we list the structure-maximizing DM (A. Seymour et al. 2019), as well as the `fitburst`-determined subburst widths, scattering timescale, and bandwidth for FRB 20241228A. As can be seen in Figure 1, the burst is visibly scattered with a timescale of 1.05 ms at 600 MHz.[26] We also determine the peak flux, specific fluence, and radio luminosity (calculated using the source's redshift and cosmological parameters from Planck Collaboration et al. 2020) for the burst by using its baseband position to correct for CHIME's instrumental beam effects (CHIME/FRB Collaboration et al. 2024).

Table 3
Burst Properties

Property	Burst A
Time of arrival (UTC)	2024-12-28 15:55:56.984
Real-time signal-to-noise	50
Baseband signal-to-noise	202
Dispersion measure	246.53 ± 0.02 pc cm^{-3}
Width	1: 0.59 ± 0.01 ms
	2: 0.533 ± 0.005 ms
Scattering timescale	1.05 ± 0.01 ms
Peak flux	41 ± 4 Jy
Fluence	140 ± 14 Jy ms
Luminosity	$3.7 \pm 0.4 \times 10^{43}$ erg s^{-1}
Bandwidth	400 MHz
Scintillation bandwidth	18 kHz

Note. Time of arrival (or TOA; topocentric) is calculated with the baseband data at 400 MHz using a DM constant of $1.0/(2.41 \times 10^{-4}$ MHz^2 s/(pc cm^{-3}). The S/N corresponds to the real-time detection S/N at a time resolution of 0.983 ms. The baseband S/N is calculated at a time resolution of 0.655 ms. The scintillation bandwidth is measured at 600 MHz.

4.2. Scintillation

Following the method outlined by K. Nimmo et al. (2025), we search for evidence of scintillation within the spectrum of FRB 20241228A. As a brief overview of the scintillation pipeline, we first upchannelize the data in frequency by performing a fast Fourier transform (FFT) to switch between the time and frequency domains. We search over a range of FFT upchannelization factors, ranging from a user-determined minimum (typically set to 16) to a maximum of 1/total burst width. For each upchannelization factor, we subband the data and examine the autocorrelation function (ACF), masking the natural zero-lag spike and normalizing such that the peak of the ACF corresponds to the square root of the modulation index. Due to reflections between CHIME's reflectors and feed lines, there is a 30 MHz frequency scale in the ACF that is not astrophysical. Additionally, a leftover upchannelization artifact can occur, which appears at 0.39 MHz. We do not attempt to remove the 30 MHz ripple, meaning we lose sensitivity to scintillation scales close to 30 MHz. We do fit a model to remove the leftover upchannelization artifact. For each subband, we fit a Lorentzian where the half-width at half-maximum corresponds to the scintillation bandwidth. To confirm that the frequency scale we measure in the ACF is from astrophysical scintillation, we search for a frequency-dependent variation in this scale, $\Delta\nu_{\mathrm{DC}} \propto \nu^{\alpha}$, that is consistent with an exponential with $\alpha \approx 4$, as expected for scintillation from a screen composed of Gaussian phase fluctuations.[27]

[26] We do not measure the scattering timescales of the individual subbursts as there is significant overlap between the scattering tail of the first with the main emission of the second.
[27] In more complex scattering configurations, the scaling of ν can be more complicated, with significantly shallower slopes in cases where one screen is resolving another.

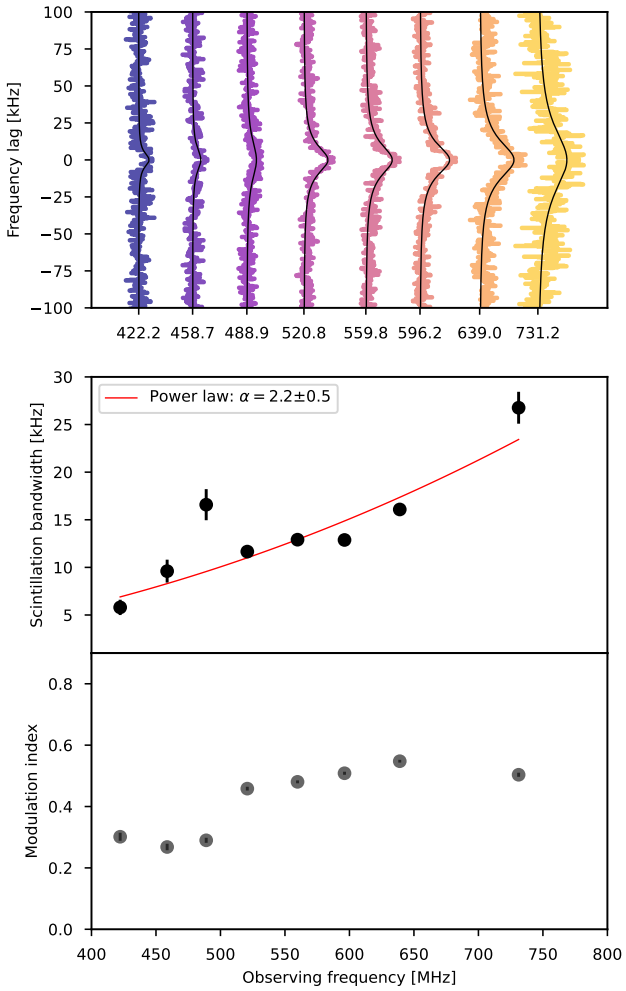

Figure 5. Top panel: ACFs for eight different subbands in the 400−800 MHz CHIME/FRB band for FRB 20241228A. The black curve shows the best-fit Lorentzian with the scintillation bandwidth corresponding to the FWHM of this function. We do not subtract the 30 MHz ripple from CHIME before calculating the ACF. However, it is much larger than the kHz structure probed here. This panel shares the same x-axis as the other two panels, but with different tick marks. Middle panel: scintillation bandwidths from the Lorentzian fits as a function of frequency. The best-fit power law is shown as a red line, and is consistent (within 3σ) with the expected $\alpha = 4$. Bottom panel: modulation index (proportional to height of ACF at zero lag) across the eight subbands. We caution that by not removing the 30 MHz ripple prior to the ACF, the absolute magnitude of the modulation indices may be affected.

For FRB 20241228A, we find the scintillation is most clearly visible at an upchannelization factor of 1024 (and hence frequency resolution of 0.7 kHz). We subband the 400–800 MHz CHIME bandwidth into eight distinct subbands with equal S/N in each band. We then determine a per-subband ACF with a Lorentzian fit (see top panel of Figure 5) over a frequency lag range of 0.6 MHz. The frequency scale observed in the ACF clearly evolves with frequency (Figure 5). We measure $\alpha = 2.2 \pm 0.5$, consistent within 3σ with the expectation of $\alpha \approx 4$ (see middle panel of Figure 5), thus suggesting this frequency scale to be astrophysical scintillation. We measure a characteristic scintillation bandwidth of 15 ± 3 kHz at 600 MHz.

The expected scintillation bandwidth from the Milky Way (MW) in this direction (Galactic latitude $\sim 3.^{\circ}5$, Galactic longitude $\sim 62.^{\circ}5$) is $\sim$200 kHz at 600 MHz (J. M. Cordes & T. J. W. Lazio 2002; S. K. Ocker & J. M. Cordes 2024). While this is approximately an order of magnitude larger than that seen in our measurements, the NE2001 model can exhibit particularly large uncertainties. The expected scattering timescale from the MW in this direction is 0.0006 ms, 3 full orders of magnitude lower than our measured scattering timescale. If we assume the scattering and scintillation measurements arise from the same source, then we would expect $2\pi\tau\Delta\nu_{\rm DC} \approx 1$. Using the $\sim$1 ms measured scattering timescale and 15 kHz scintillation scale, we find $2\pi\tau\Delta\nu_{\rm DC} \approx 100$, significantly larger than 1. This means that the scattering screen responsible for the 1.05 ms measured scattering in FRB 20241228A is distinct from the 15 kHz scintillation screen along this source's line of sight. While both our scintillation and scattering measurements are discrepant with that predicted by NE2001, the scintillation measurement is in closer agreement (1 order of magnitude) while the scattering measurement is in clear disagreement (3 orders of magnitude). While both screens could be Galactic, this is unlikely as the dominant scattering screen would resolve the scintillation screen, and hence only scintillation features from the scattering screen would be detectable. Hence, we conclude that the scintillation screen is likely Galactic, while the scattering screen is likely extragalactic.

The strength of the scintillation screen is quantified through the modulation index, where in our case the modulation index is equal to the square root of the amplitude of the Lorentzian fit to each ACF. However, the absolute amplitude of the modulation indices measured is complicated by the remnant 30 MHz ripple, as well as any remaining upchannelization artifacts. Future work will explore in detail the impact of these artifacts on our measured modulation indices. As a conservative approach, we present the constraints for both the case in which the emission is fully modulated yet reduced due to systematics, as well that in which the modulation index is indeed less than 1.

Assuming the emission is fully modulated and that there are two distinct screens along the line of sight to this source, we use Equation (7.6) from E. T. S. Pradeep et al. (2025) with $\nu_{\rm DC} = 15$ kHz, $\nu = 600$ MHz, and $\tau = 1.05$ ms to constrain $d_1 d_2 \lesssim 14$ kpc^2, where d_1 is the distance between us and the Galactic screen and d_2 is the distance between the extragalactic screen and the FRB. Using the updated NE2001p model, we estimate that the Galactic scintillation screen is located at $d_1 = 0.522$ kpc by searching for the maximum amplitude of the electron density fluctuation power spectrum (C_n^2) along the line of sight (J. M. Cordes & T. J. W. Lazio 2002; S. K. Ocker & J. M. Cordes 2024). Given this Galactic screen distance, the extragalactic screen would be at $d_2 < 28$ kpc from the FRB. This is, however, highly dependent on the estimated Galactic scintillation screen distance. The furthest screen found off the Galactic plane is at a scale height of $\sim$2 kpc (T. Sprenger et al. 2022). Thus, for a Galactic screen at a distance of 2 kpc, $d_2 < 7$ kpc. In both cases, this is consistent with the expectation that the FRB and the screen are within the disk/halo of the host galaxy.

While the above result seems the most astrophysically likely (fully modulated, screen within the host galaxy), it remains possible that the modulation index is indeed less than 1. Assuming one screen is partially resolving the other, we find $d_1 d_2 = \frac{14 \mathrm{kpc}^2}{m}$, where m is the modulation index. Given $m = 0.4$ (average across all frequency bins) and $d_1 = 0.5$, this gives a distance of $\sim$35 kpc between the FRB and extragalactic screen. In this case, the FRB might be located behind the Galaxy itself,

or the scattering screen might be located within the circumgalactic medium. However, further interpretation of this requires a detailed investigation of the systematics affecting our modulation index.

4.3. Polarimetry

We determine the polarimetry of the burst following the pipeline developed by R. Mckinven et al. (2021). The source has a Faraday rotation measure (RM) of -38.64 ± 0.01 rad m^{-2}, with a linear polarization fraction of 85.3% ± 0.4%. The inferred Galactic RM contribution along this line of sight is 8 ± 5 rad m^{-2} (S. Hutschenreuter et al. 2022). It does not exhibit any swings in its polarization angle as a function of time (see Figure 6 in the Appendix).

4.4. Rate

Following the method presented by CHIME/FRB Collaboration et al. (2021), we calculate the total exposure within the full width half-maximum of the CHIME/FRB-formed beams at the location of this source to be 119 hr. Using the exposure, source position, and fluence, we calculate a spectral fluence threshold following the method outlined by A. Josephy et al. (2019). The 68th percentile of the fluence threshold distribution is 18.8 Jy ms, while the 95th percentile is 29 Jy ms. We scale the burst rate, <0.008 burst hr^{-1}, to a fluence threshold of 5 Jy ms assuming a power-law index of −1.5 for the cumulative energy distribution (CHIME/FRB Collaboration et al. 2023) and using the 95th percentile fluence threshold. The upper limit on the burst rate is 0.12 burst hr^{-1} above a fluence threshold of 5 Jy ms.

5. Discussion and Summary

In this work, we provide the localization and burst property analysis for the thus far nonrepeating FRB 20241228A. This source is special, as Swift/XRT was on target at the source position only 112 s after the burst (A. Tohuvavohu et al. 2026, in preparation), representing the fastest X-ray trigger for a nonrepeating FRB to date. A. Tohuvavohu et al. (2026, in preparation) present an upper limit on the persistent X-ray flux of 1.52×10^{-13} erg cm^{-2} s^{-1} in the 0.3−10 keV band 112 s after the FRB. Using CHIME/FRB along with the GBO and KKO Outriggers, we obtained a VLBI-level localization for FRB 20241228A and robustly associated it with a host galaxy at a redshift of $z = 0.1614$. At this redshift, and assuming cosmology from Planck Collaboration et al. (2020), this corresponds to an X-ray luminosity limit of 1.2×10^{43} erg s^{-1}. Given the radio luminosity presented in Table 3, this corresponds to $L_x/L_r < 1$.

In this work, we explore the host galaxy and burst properties of FRB 20241228A. It is found in a spiral star-forming galaxy, consistent with what is found for most FRB host galaxies (e.g., M. Bhardwaj et al. 2024). Indeed, while the measured SFR is on the higher end when compared to those in A. C. Gordon et al. (2023), the stellar mass is also commensurately high, leading to a specific star formation rate right at the median value of the full sample. Thus, overall the host-galaxy properties of FRB 20241228A resemble those of the broader FRB host population.

We did not find any other bursts within the CHIME/FRB database at the location of FRB 20241228A. The source's full 400 MHz bandwidth closely resembles that of the nonrepeating FRB population, further supporting its classification as a nonrepeater (Z. Pleunis 2021; K. R. Sand et al. 2025). However, the upper limit on the source's rate (0.12 burst hr^{-1}) is consistent with that of most repeating FRBs detected by CHIME/FRB (CHIME/FRB Collaboration et al. 2023; A. P. Curtin et al. 2025), and the source's duration (∼1 ms) is consistent with both the repeating and nonrepeating populations reported in K. R. Sand et al. (2025) and A. P. Curtin et al. (2025). Additionally, the lifetime of FRBs is highly uncertain, and thus FRB 20241228A may just be entering its active phase.

FRB 20241228A represents an unique and exciting example of a new era in FRB science: coordinated, rapid X-ray follow-up and subarcsecond VLBI localizations. With the addition of the third CHIME/FRB Outrigger, we will be able to pinpoint FRBs on ∼50 mas-level scales (CHIME/FRB Collaboration et al. 2025c). Combined with deep, rapid X-ray observations, this capability will enable stringent constraints on FRB progenitor models and their local environments.

Acknowledgments

We acknowledge that CHIME and the k'niʔatn k'l⌣stk'masqt Outrigger (KKO) are built on the traditional, ancestral, and unceded territory of the Syilx Okanagan people. K'niʔatn k'l⌣stk'masqt is situated on land leased from the Imperial Metals Corporation. We are grateful to the staff of the Dominion Radio Astrophysical Observatory, which is operated by the National Research Council of Canada. CHIME operations are funded by a grant from the NSERC Alliance Program and by support from McGill University, University of British Columbia, and University of Toronto. CHIME/FRB Outriggers are funded by a grant from the Gordon & Betty Moore Foundation. We are grateful to Robert Kirshner for early support and encouragement of the CHIME/FRB Outriggers Project, and to Dusan Pejakovic of the Moore Foundation for continued support. CHIME was funded by a grant from the Canada Foundation for Innovation (CFI) 2012 Leading Edge Fund (Project 31170) and by contributions from the provinces of British Columbia, Québec, and Ontario. The CHIME/FRB Project was funded by a grant from the CFI 2015 Innovation Fund (Project 33213) and by contributions from the provinces of British Columbia and Québec, and by the Dunlap Institute for Astronomy and Astrophysics at the University of Toronto. Additional support was provided by the Canadian Institute for Advanced Research (CIFAR), the Trottier Space Institute at McGill University, and the University of British Columbia. The CHIME/FRB raw voltage data recording system is funded in part by a CFI John R. Evans Leaders Fund award to IHS.

A.P.C. is a Canadian SKA Scientist and is funded by the Government of Canada/est financé par le gouvernement du Canada. S.S. is supported by the joint Northwestern University and University of Chicago Brinson Fellowship. K.N. is an MIT Kavli Fellow. A.M.C. is a Banting Postdoctoral Researcher. F. A.D. is an NRAO Jansky Fellow. Y.D. is supported by the National Science Foundation Graduate Research Fellowship under grant No. DGE-2234667. W.F. gratefully acknowledges support by the David and Lucile Packard Foundation, the Research Corporation for Science Advancement through Cottrell Scholar Award #28284, and the NSF (grant No. AST-2206494, CAREER grant AST-2047919). E.F. is supported by the National Science Foundation (NSF) under grant No. AST-2407399. J.W.T.H. and the AstroFlash research group acknowledge support from a Canada Excellence

Research Chair in Transient Astrophysics (CERC-2022-00009), an Advanced Grant from the European Research Council (ERC) under the European Union's Horizon 2020 research and innovation program ("EuroFlash"; grant agreement No. 101098079), and an NWO-Vici grant ("AstroFlash"; VI.C.192.045). V.M.K. holds the Lorne Trottier Chair in Astrophysics and Cosmology, a Distinguished James McGill Professorship, and receives support from an NSERC Discovery grant (RGPIN 228738-13). C. L. acknowledges support from the Miller Institute for Basic Research at UC Berkeley. K.W.M. holds the Adam J. Burgasser Chair in Astrophysics and is supported by NSF grant No. 2018490. D.M. acknowledges support from the French government under the France 2030 investment plan, as part of the Initiative d'Excellence d'Aix-Marseille Université – A*MIDEX (AMX-23-CEI-088). M.N. is a Fonds de Recherche du Quebec – Nature et Technologies (FRQNT) postdoctoral fellow. A.P. is funded by the NSERC Canada Graduate Scholarships – Doctoral program. A.B.P. is a Banting Fellow, a McGill Space Institute (MSI) Fellow, and a Fonds de Recherche du Quebec – Nature et Technologies (FRQNT) postdoctoral fellow. Z.P. is supported by an NWO Veni fellowship (VI.Veni.222.295). M.W.S. acknowledges support from the Trottier Space Institute Fellowship program. K.R.S is supported by a FRQNT doctoral research award. P.S. acknowledges the support of an NSERC Discovery Grant (RGPIN-2024-06266). V.S. is supported by a FRQNT doctoral research award. K.S. is supported by the NSF Graduate Research Fellowship Program.

Facilities: CHIME, Gemini:Gillett

Software: `Fitburst`, `PATH`, `ffff-pz`, `Marz`, `CIGALE`.

Appendix

In Figure 6, we show the polarization for the primary subburst of FRB 20241228A.

In Table 4, we list the photometric surveys used to create the SED shown in Figure 7 for the host galaxy of FRB 20241228A.

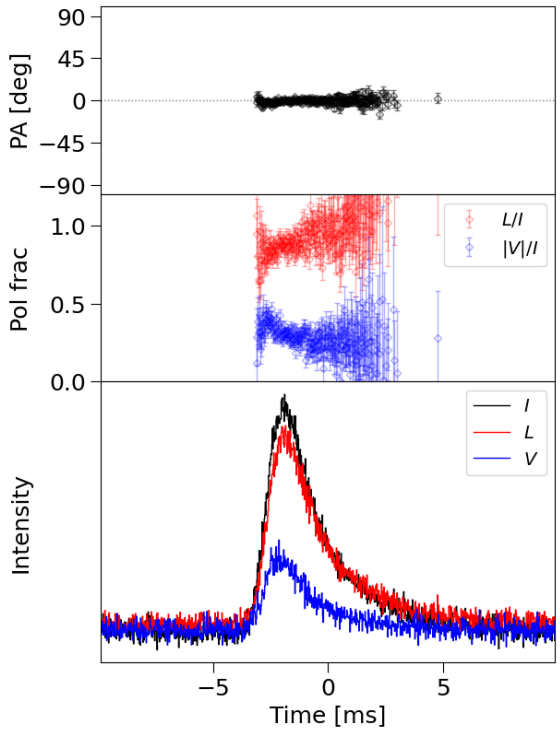

Figure 6. Fractional linear and circular polarization for FRB 20241228A. We do not show the first, weaker subburst as the linearly polarized S/N is less than 5. Top panel: polarization angle (PA) over the primary subburst of FRB 20241228A. The burst is dedispersed to the structure-maximizing DM presented in Table 3, and the data are at a time resolution of 81.92 μs. Middle panel: linear (L/I) and circular ($|V|/I$) polarization fractions. Bottom panel: linear and circular polarization profile as compared to the full intensity profile.

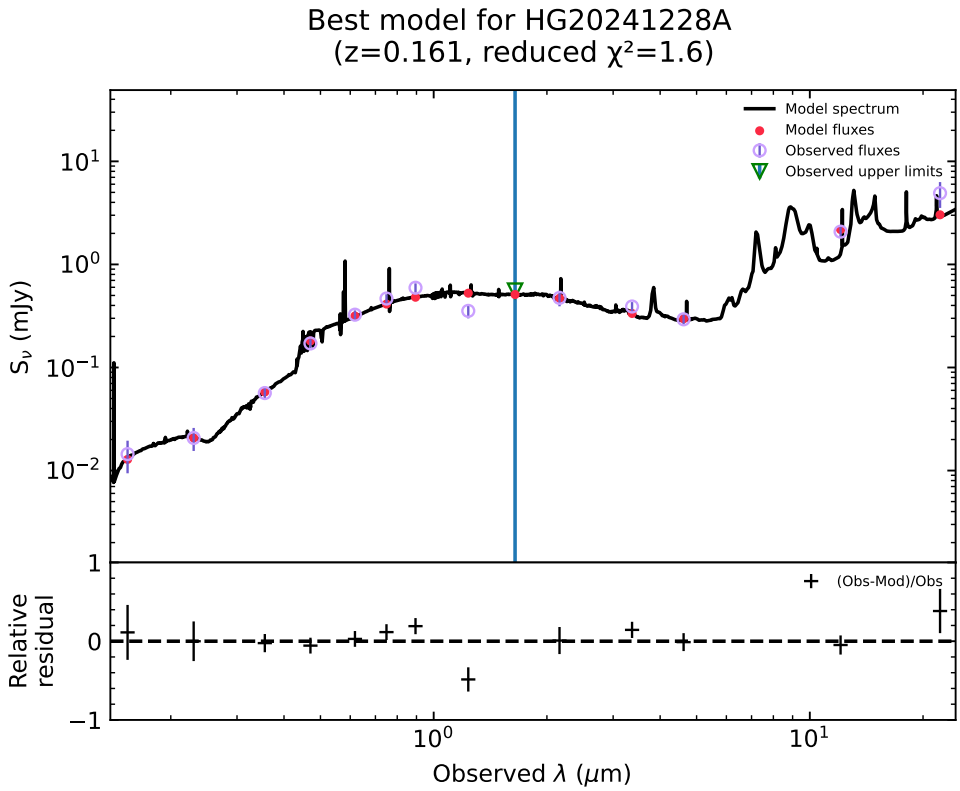

Figure 7. SED fit for the host-galaxy photometry (purple circles with error bars) using CIGALE. The black line shows the best model fit and is composed of various model components (colored lines). The input photometry is from the Pan-STARRS, SDSS, DELVE, DECaLS, and WISE databases. See Table 4 for photometry values.

Table 4
Extinction-corrected Optical Photometry of the Host Galaxy Obtained from GALEX, SDSS, 2MASS, and WISE

Survey	Band	Mag (AB)
GALEX	FUV	21.0 ± 0.4
	NUV	20.6 ± 0.2
SDSS	*u*	19.52 ± 0.06
	g	18.32 ± 0.01
	r	17.619 ± 0.009
	i	17.228 ± 0.009
	z	16.96 ± 0.02
2MASS	*J*	17.5 ± 0.1
	H	> 17
	K	17.2 ± 0.2
WISE	W1	17.42 ± 0.03
	W2	17.73 ± 0.06
	W3	15.60 ± 0.08
	W4	14.7 ± 0.3

ORCID iDs

Alice P. Curtin https://orcid.org/0000-0002-8376-1563
Shion Andrew https://orcid.org/0000-0002-3980-815X
Sunil Simha https://orcid.org/0000-0003-3801-1496
Alice Cai https://orcid.org/0009-0001-0983-623X
Kenzie Nimmo https://orcid.org/0000-0003-0510-0740
Shami Chatterjee https://orcid.org/0000-0002-2878-1502
Amanda M. Cook https://orcid.org/0000-0001-6422-8125
Fengqiu Adam Dong https://orcid.org/0000-0003-4098-5222
Yuxin Dong https://orcid.org/0000-0002-9363-8606
Tarraneh Eftekhari https://orcid.org/0000-0003-0307-9984
Wen-fai Fong https://orcid.org/0000-0002-7374-935X
Emmanuel Fonseca https://orcid.org/0000-0001-8384-5049
Jason W. T. Hessels https://orcid.org/0000-0003-2317-1446
Ronniy C. Joseph https://orcid.org/0000-0003-3457-4670
Victoria Kaspi https://orcid.org/0000-0001-9345-0307
Calvin Leung https://orcid.org/0000-0002-4209-7408
Robert Main https://orcid.org/0000-0002-7164-9507
Kiyoshi W. Masui https://orcid.org/0000-0002-4279-6946
Ryan Mckinven https://orcid.org/0000-0001-7348-6900
Daniele Michilli https://orcid.org/0000-0002-2551-7554
Mason Ng https://orcid.org/0000-0002-0940-6563
Ayush Pandhi https://orcid.org/0000-0002-8897-1973
Aaron B. Pearlman https://orcid.org/0000-0002-8912-0732
Mawson W. Sammons https://orcid.org/0000-0002-4623-5329
Ketan R Sand https://orcid.org/0000-0003-3154-3676
Paul Scholz https://orcid.org/0000-0002-7374-7119
Vishwangi Shah https://orcid.org/0000-0002-4823-1946
Kaitlyn Shin https://orcid.org/0000-0002-6823-2073
Aaron Tohuvavohu https://orcid.org/0000-0002-2810-8764

References

Abbott, T. C., Zwaniga, A. V., Brar, C., et al. 2025, AJ, 169, 39
Aggarwal, K., Budavári, T., Deller, A. T., et al. 2021, ApJ, 911, 95
Andrew, S., Leung, C., Li, A., et al. 2025, ApJ, 981, 39
Anumarlapudi, A., Bhalerao, V., Tendulkar, S. P., & Balasubramanian, A. 2020, ApJ, 888, 40
Bhardwaj, M., Michilli, D., Kirichenko, A. Y., et al. 2024, ApJL, 971, L51
Bianchi, L., Shiao, B., & Thilker, D. 2017, ApJS, 230, 24

Bochenek, C. D., Ravi, V., Belov, K. V., et al. 2020, Natur, 587, 59
Boquien, M., Burgarella, D., Roehlly, Y., et al. 2019, A&A, 622, A103
Brisken, W. F., Benson, J. M., Goss, W. M., & Thorsett, S. E. 2002, ApJ, 571, 906
Bruzual, G., & Charlot, S. 2003, MNRAS, 344, 1000
Calzetti, D. 2001, PASP, 113, 1449
Cappellari, M. 2017, MNRAS, 466, 798
Casentini, C., Verrecchia, F., Tavani, M., et al. 2020, ApJL, 890, L32
Chabrier, G. 2003, PASP, 115, 763
Chambers, K. C., Magnier, E., Metcalfe, N., et al. 2016, arXiv:1612.05560
Chatterjee, S., Brisken, W. F., Vlemmings, W. H. T., et al. 2009, ApJ, 698, 250
CHIME/FRB Collaboration, Amiri, M., Bandura, K., et al. 2018, ApJ, 863, 48
CHIME/FRB Collaboration, Andersen, B. C., Bandura, K. M., et al. 2020a, Natur, 587, 54
CHIME/FRB Collaboration, Amiri, M., Andersen, B. C., et al. 2020b, Natur, 582, 351
CHIME/FRB Collaboration, Amiri, M., Andersen, B. C., et al. 2021, ApJS, 257, 59
CHIME/FRB Collaboration, Andersen, B. C., Bandura, K., et al. 2023, ApJ, 947, 83
CHIME/FRB Collaboration, Amiri, M., Andersen, B. C., et al. 2024, ApJ, 969, 145
CHIME/FRB Collaboration, Amiri, M., Andersen, B. C., et al. 2025a, ApJ, 993, 55
CHIME/FRB Collaboration, Amiri, M., Amouyal, D., et al. 2025b, ApJS, 280, 6
CHIME/FRB Collaboration, Abbott, T. C., Amouyal, D., et al. 2025c, ApJL, 989, L48
CHIME/FRB Collaboration, Abbott, T., & Anderson, B. C. 2026, arXiv:2601.09399
Conroy, C., Gunn, J. E., & White, M. 2009, ApJ, 699, 486
Cook, A. M., Scholz, P., Pearlman, A. B., et al. 2024, ApJ, 974, 170
Cordes, J. M., & Lazio, T. J. W. 2002, arXiv:astro-ph/0207156
Coulter, D. A., Jones, D. O., McGill, P., et al. 2022, YSE-PZ: An Open-source Target and Observation Management System, v0.3.0, Zenodo, doi:10.5281/zenodo.7278430
Coulter, D. A., Jones, D. O., McGill, P., et al. 2023, PASP, 135, 064501
Curtin, A. P. & CHIME/FRB Collaboration 2023, ATel, 16341, 1
Curtin, A. P., Tendulkar, S. P., Josephy, A., et al. 2023, ApJ, 954, 154
Curtin, A. P., Sirota, S., Kaspi, V. M., et al. 2024, ApJ, 972, 125
Curtin, A. P., Sand, K. R., Pleunis, Z., et al. 2025, ApJ, 992, 206
Dale, D. A., Helou, G., Magdis, G. E., et al. 2014, ApJ, 784, 83
Deller, A. T., Goss, W. M., Brisken, W. F., et al. 2019, ApJ, 875, 100
Dey, A., Schlegel, D. J., Lang, D., et al. 2019, AJ, 157, 168
Drlica-Wagner, A., Carlin, J. L., Nidever, D. L., et al. 2021, ApJS, 256, 2
Eftekhari, T., Fong, W., Gordon, A. C., et al. 2023, ApJ, 958, 66
Eftekhari, T., Dong, Y., Fong, W., et al. 2025, ApJL, 979, L22
Fonseca, E., Pleunis, Z., Breitman, D., et al. 2024, ApJS, 271, 49
Gehrels, N., Chincarini, G., Giommi, P., et al. 2004, ApJ, 611, 1005
Gordon, A. C., Fong, W. F., Kilpatrick, C. D., et al. 2023, ApJ, 954, 80
Gordon, A. C., Fong, W. F., Deller, A. T., et al. 2025, ApJ, 993, 119
Guidorzi, C., Marongiu, M., Martone, R., et al. 2020, A&A, 637, A69
Hardy, L. K., Dhillon, V. S., Spitler, L. G., et al. 2017, MNRAS, 472, 2800
Hinton, S., Davis, T. M., Lidman, C., Glazebrook, K., & Lewis, G. 2016, A&C, 15, 61
Hiramatsu, D., Berger, E., Metzger, B. D., et al. 2023, ApJL, 947, L28
Hutschenreuter, S., Anderson, C. S., Betti, S., et al. 2022, A&A, 657, A43
Josephy, A., Chawla, P., Fonseca, E., et al. 2019, ApJL, 882, L18
Kennicutt, R. C., Jr. 1998, ApJ, 498, 541
Kilpatrick, C. D., Tejos, N., Andersen, B. C., et al. 2024, ApJ, 964, 121
Lanman, A. E., Andrew, S., Lazda, M., et al. 2024, AJ, 168, 87
Leung, C., Mena-Parra, J., Masui, K., et al. 2021, AJ, 161, 81
Leung, C., Andrew, S., Masui, K. W., et al. 2025, AJ, 170, 53
Li, C. K., Lin, L., Xiong, S. L., et al. 2021, NatAs, 5, 378
Lin, H.-H., Scholz, P., Ng, C., et al. 2024, ApJ, 975, 75
Lin, R., van Kerkwijk, M. H., Kirsten, F., Pen, U.-L., & Deller, A. T. 2023, ApJ, 952, 161
Mckinven, R., Michilli, D., Masui, K., et al. 2021, ApJ, 920, 138
Mereghetti, S., Savchenko, V., Ferrigno, C., et al. 2020, ApJL, 898, L29
Michilli, D., Masui, K. W., Mckinven, R., et al. 2021, ApJ, 910, 147
Morrissey, P., Conrow, T., Barlow, T. A., et al. 2007, ApJS, 173, 682
Ng, C., Vanderlinde, K., Paradise, A., et al. 2017, in Proc. XXXII URSI GAS (IEEE), 4
Nimmo, K., Pleunis, Z., Beniamini, P., et al. 2025, Natur, 637, 48
Ocker, S. K., & Cordes, J. M. 2024, RNAAS, 8, 17
Osterbrock, D. E., & Ferland, G. J. 2006, Astrophysics of Gaseous Nebulae and Active Galactic Nuclei (2nd ed.; University Science Books)
Palmer, D. M. & Swift/BAT Team 2020, ATel, 13675, 1
Pearlman, A. B., Scholz, P., Bethapudi, S., et al. 2025, NatAs, 9, 111
Peng, C. Y., Ho, L. C., Impey, C. D., & Rix, H.-W. 2002, AJ, 124, 266
Petroff, E., Houben, L., Bannister, K., et al. 2017, arXiv:1710.08155
Pilia, M., Burgay, M., Possenti, A., et al. 2020, ApJL, 896, L40
Piro, L., Bruni, G., Troja, E., et al. 2021, A&A, 656, L15
Planck Collaboration, Aghanim, N., Akrami, Y., et al. 2020, A&A, 641, A6
Pleunis, Z. 2021, PhD thesis, McGill University
Pradeep, E. T. S., Sprenger, T., Wucknitz, O., Main, R. A., & Spitler, L. G. 2025, A&A, 700, A99
Prochaska, J. X., Hennawi, J., Cooke, R., et al. 2020, pypeit/PypeIt: Release, v1.0.0, Zenodo, doi:10.5281/zenodo.3743493
Rajwade, K. M., Mickaliger, M. B., Stappers, B. W., et al. 2020, MNRAS, 495, 3551
Ridnaia, A., Svinkin, D., Frederiks, D., et al. 2021, NatAs, 5, 372
Rodrigo, C., & Solano, E. 2020, XIV.0 Scientific Meeting (virtual) of the Spanish Astronomical Society, 182
Rodrigo, C., Cruz, P., Aguilar, J. F., et al. 2024, A&A, 689, A93
Sand, K. R., Curtin, A. P., Michilli, D., et al. 2025, ApJ, 979, 160
Schlafly, E. F., & Finkbeiner, D. P. 2011, ApJ, 737, 103
Scholz, P., Bogdanov, S., Hessels, J. W. T., et al. 2017, ApJ, 846, 80
Scholz, P., Cook, A., Cruces, M., et al. 2020, ApJ, 901, 165
Seymour, A., Michilli, D., & Pleunis, Z., 2019 DM_phase: Algorithm for correcting dispersion of radio signals, Astrophysics Source Code Library, ascl:1910.004
Shah, V., Shin, K., Leung, C., et al. 2025, ApJL, 979, L21
Simha, S., Burchett, J. N., Prochaska, J. X., et al. 2020, ApJ, 901, 134
Sprenger, T., Main, R., Wucknitz, O., Mall, G., & Wu, J. 2022, MNRAS, 515, 6198
Tendulkar, S. P., Kaspi, V. M., & Patel, C. 2016, ApJ, 827, 59
Tohuvavohu, A., Kennea, J. A., DeLaunay, J., et al. 2020, ApJ, 900, 35
Trudu, M., Pilia, M., Nicastro, L., et al. 2023, A&A, 676, A17
Waratkar, G., Dixit, M., Tendulkar, S. P., et al. 2025, JApA, 46, 59
Wright, E. L., Eisenhardt, P. R., Mainzer, A. K., et al. 2010, AJ, 140, 1868
Yamasaki, S., Totani, T., & Kawanaka, N. 2016, MNRAS, 460, 2875
Yan, Z., Yu, W., Page, K. L., et al. 2025, ApJ, 983, 116
Yao, J. M., Manchester, R. N., & Wang, N. 2017, ApJ, 835, 29
York, D. G., Adelman, J., Anderson, J. E., Jr., et al. 2000, AJ, 120, 1579